PHYSICAL REVIEW A VOLUME 50, NUMBER 2 AUGUST 1994

Exponential gain and self-bunching in a collective atomic recoil laser

R. Bonifacio and L. De Salvo
Dipartimento di Fisica, Universitá di Milano and Istituto Nazionale di Fisica Nucleare, Via Celoria 16, 20133 Milano, Italy

L. M. Narducci and E. J. D'Angelo
Physics Department, Drexel University, Philadelphia, Pennsylvania 19104
(Received 14 February 1994)

We show how a collection of noninverted two-level systems, under the action of a quasiresonant pump field, can produce an exponential amplification of a probe signal through the mechanism of a dynamical instability with spatial self-bunching in a way very similar to that experienced by a high-gain free-electron laser. We offer a detailed description of this phenomenon, specify the conditions under which it takes place, and sketch possible experimental parameters for its observation in a gaseous medium.

PACS number(s): 42.55.−f, 42.50.−p, 32.80.Pj

I. INTRODUCTION

The two best known sources of coherent radiation, the ordinary laser and the free-electron laser (FEL), share an important physical trait: they generate electromagnetic waves through a noise-initiated process of self-organization. For the rest, however, their modes of operation are different enough that one may even question the wisdom of using the term "laser" in conjunction with the FEL. In an ordinary laser, for example, the energy is stored initially as excitation of internal degrees of freedom of the active medium, while in a free-electron laser it is brought into the interaction region as translational kinetic energy of the incident electron beam. The spectral character of laser light is constrained mainly by the gain profile of the active medium, while in a free-electron laser the frequency of the emitted radiation is assigned by the speed of the incident electrons, and can be varied, in principle, over a very wide range; hence, the FEL is intrinsically a widely tunable source. Furthermore, the laser gain originates from the induced atomic polarization, under the constraint that a suitable population inversion exists in the active medium; in a free-electron laser, instead, amplification of coherent radiation follows the spontaneous emergence of a sufficiently large electron bunching, i.e., the appearance of a periodic spatial structure in the form of a longitudinal grating on the scale of the electromagnetic wavelength. Hence, light amplification in a FEL is the result of a coherent scattering process from the grating structure created within the active medium, and it comes at the expense of a recoil in the momentum of the individual electrons.

In this paper we describe a source of tunable coherent radiation, the collective atomic recoil laser (CARL), a kind of hybrid between the FEL and the ordinary laser, with physical features common to both. Its essential conceptual framework was outlined in Ref. [1]; here we discuss, in additional details, the basic features of this system and its operating principles, we make some specific predictions, and offer a preliminary analysis for an experimental proof of principle.

We visualize the active medium of this new source of coherent radiation as a beam of two-level atoms [2]. The atoms, initially in the lower state of the laser transition, are driven by a counterpropagating light field near or on resonance with their Doppler-shifted transition frequency, and for appropriate values of the parameters they can amplify a weak copropagating field through an exponential instability which is reminiscent of the threshold behavior of a free-electron laser [3].

This system unifies many aspects of the physics of the FEL and of the atomic laser in a mode of operation that does not require the initial preparation of a state of population inversion, a feature that is also common to the so-called inversionless lasers [4]. As in the laser, the active medium is characterized by bound states which play a key role in the amplification process, as we show in the main body of this paper, but do not possess a population inversion. Common to the FEL, instead, is the existence of a reservoir of momentum that can be transformed partly into radiation through a kind of cooperative Compton scattering. Furthermore, optical gain is initiated by the growth of a bunching parameter.

Perhaps one of the most singular features of the CARL system is the combined role played in the amplification process by the small signal response of the driven atoms and by the atomic recoil. In fact, in the early stages of the evolution the response of the driven atoms to a weak probe matches qualitatively some of the gain and absorption features predicted by Mollow for stationary driven systems [5], hence, it displays symmetric gain sidebands when the driving field is resonant with the atomic transition and the Raman gain peak and absorption dip, otherwise. However, it also shows the characteristic antisymmetric Madey gain [6] of the free-electron laser when the Doppler-shifted pump and probe frequencies coincide. This latter feature is a characteristic effect of the atomic recoil; moreover, because the translational degrees of freedom are built into the model, the Madey gain profile becomes more pronounced and loses its antisymmetric shape as the momentum of the atoms decreases. Selecting the probe frequency in correspondence to the Madey

1050-2947/94/50(2)/1716(9)/$06.00

gain feature yields strong exponential amplification further into the evolution. This aspect of the problem is unique to this system, as far as we know.

This paper is organized as follows. In Sec. II we discuss the details of the model and derive the equations of motion; in Sec. III we present selected results and interpret their physical significance; finally in Sec. IV we summarize our conclusions, comment on some recent work by Courtois and co-workers [7], and give a preliminary estimate of the CARL parameters for a selected gaseous medium.

II. DISCUSSION OF THE MODEL AND EQUATIONS OF MOTION

Our model is based on the Hamiltonian of a collection of two-level atoms interacting with a counterpropagating driving field (the pump), having prescribed amplitude and carrier frequency, and a copropagating optical probe. In addition to the internal atomic degrees of freedom, which are typical of laser models, we take explicit account of the center-of-mass motion, whose role in the light amplification process is just as important, as already stated. The explicit form of the Hamiltonian is

$$H=\hbar\omega_1 a_1^\dagger a_1+\hbar\omega_2 a_2^\dagger a_2+\hbar\omega_0\sum_{j=1}^{N}S_{zj}+\sum_{j=1}^{N}\frac{p_j^2}{2m}+i\hbar\left[g_1 a_1^\dagger\sum_{j=1}^{N}S_j^- e^{-ik_1 z_j}+g_2 a_2^\dagger\sum_{j=1}^{N}S_j^- e^{ik_2 z_j}-\text{H.a.}\right], \tag{2.1}$$

where N is the number of atoms in the interaction volume V, $\omega_{1,2}=ck_{1,2}$ are the carrier frequencies of the probe and pump fields, respectively, k_1 and k_2 are the corresponding wave numbers, and ω_0 is the atomic transition frequency when the atoms are at rest relative to the observer; g_i $(i=1,2)$ are the couplings constants, defined as $\mu[\omega_i/(2\hbar\varepsilon_0 V)]^{1/2}$, and μ is the modulus of the atomic dipole moment. S_{zj} and $S_j^\pm$ are the standard effective angular-momentum operators (in units of $\hbar$) describing the evolution of the internal degrees of freedom of the jth atom (thus, S_{zj} measures one-half the difference between the excited- and ground-state populations of the jth atom); z_j and p_j denote, respectively, the position and momentum operators of the center of mass of the jth atom and $a_i^\dagger$ $(i=1,2)$ are the photon creation operators of the copropagating field (index 1) and of the counterpropagating driving field (index 2). The operators obey the usual commutation relations.

The Hamiltonian (2.1) admits two constants of the motion,

$$\sum_{j=1}^{N}p_j+\hbar k_1 a_1^\dagger a_1-\hbar k_2 a_2^\dagger a_2=\text{const}\ , \tag{2.2a}$$

$$\sum_{j=1}^{N}S_{zj}+a_1^\dagger a_1+a_2^\dagger a_2=\text{const}\ ; \tag{2.2b}$$

the first represents the conservation of the total momentum and the second the conservation of the number of excitations. If we combine Eqs. (2.2a) and (2.2b) and eliminate the number operator of the driving field, $a_2^\dagger a_2$, we can also write

$$\sum_{j=1}^{N}(p_j+\hbar k_2 S_{zj})+\hbar(k_1+k_2)a_1^\dagger a_1=\text{const}\ , \tag{2.3}$$

whose obvious physical implication is that the expectation value of the number operator for the probe field, $a_1^\dagger a_1$, can grow either as the result of a loss of internal atomic energy or a decrease of the center-of-mass kinetic energy. This setting represents a generalization of the basic mechanisms by which energy is produced in the laser and in the FEL; in fact, the laser Hamiltonian does not involve the momentum and position operators p_j and z_j, while the FEL Hamiltonian does not include the angular-momentum operators, descriptive of the internal degrees of freedom of the active medium.

In this paper we analyze the dynamical evolution of the coherent atomic recoil laser within the framework of the standard semiclassical approximation. Thus, we first construct the Heisenberg equations of motion for the relevant operators, map the operator equations into their c-number counterparts in the usual factorized form, and finally introduce appropriate, slowly varying variables [8].

This program is accomplished by introducing the slowly varying variables a_1^0, a_2^0, and S_j according to the definitions

$$a_1(t)=a_1^0(t)\exp\left[-i\left[\omega_2+\frac{k_1+k_2}{m}\bar{p}(0)\right]t\right], \tag{2.4a}$$

$$a_2(t)=a_2^0\exp(-i\omega_2 t)\ , \tag{2.4b}$$

$$S_j^-(t)=S_j(t)\exp[-ik_2(z_j+ct)]\ , \tag{2.4c}$$

where $\bar{p}(0)\equiv m\bar{v}(0)$ is the average initial momentum of the incident atoms. Furthermore, we define the new position and momentum variables $\theta_j(t)$ and $\delta p_j(t)$,

$$\theta_j(t)=(k_1+k_2)\left[z_j(t)-\frac{\bar{p}(0)}{m}t\right], \tag{2.4d}$$

$$\delta p_j(t)=p_j(t)-\bar{p}(0)\ , \tag{2.4e}$$

and the population difference between the ground and excited states of the jth atom,

$$D_j(t)=-2S_{zj}(t)\ . \tag{2.4f}$$

Finally, the required equations of motion take the form

$$\frac{d\theta_j}{dt}=\frac{k_1+k_2}{m}\delta p_j\ , \tag{2.5a}$$

$$\frac{d}{dt}\delta p_j=-\hbar k_1 g_1 a_1^{0*}S_j e^{-i\theta_j}+\hbar k_2 g_2 a_2^{0*}S_j+\text{c.c.}\ , \tag{2.5b}$$

$$\frac{da_1^0}{dt}=i\delta_{2,1}a_1^0+g_1\sum_{j=1}^{N}S_j e^{-i\theta_j}\ , \tag{2.5c}$$

$$\frac{dS_j}{dt}=i\left[\frac{\omega_2}{c}\frac{\delta p_j}{m}+\delta_{2,0}\right]S_j-g_1a_1^0D_je^{i\theta_j}-g_2a_2^0D_j -\gamma_\perp S_j \;, \tag{2.5d}$$

$$\frac{dD_j}{dt}=(2g_1a_1^{0*}S_je^{-i\theta_j}+2g_2a_2^{0*}S_j+\text{c.c.}) -\gamma_\parallel(D_j-D_j^{\text{eq}}) \;, \tag{2.5e}$$

where we have introduced the detuning parameters

$$\delta_{2,1}=(k_1+k_2)[\bar{v}(0)-v_{r,1}] \;, \tag{2.6a}$$

$$\delta_{2,0}=k_2[\bar{v}(0)-v_{r,2}] \;, \tag{2.6b}$$

with

$$v_{r,1}=\frac{\omega_1-\omega_2}{\omega_1+\omega_2}c \;, \quad v_{r,2}=\frac{\omega_0-\omega_2}{\omega_2}c \;, \tag{2.6c}$$

and added phenomenological decay terms to the polarization and population equations (D_j^{eq} is the equilibrium population difference in the absence of both driving and probe beams; in our case, $D_j^{\text{eq}}=1$ because each incident atom is assumed to be in the ground state as it enters the interaction region). Note that the two resonance conditions $\delta_{2,0}=\delta_{2,1}=0$, taken together, imply

$$\omega_1=\frac{\omega_0}{1-\beta_0} \;, \quad \omega_2=\frac{\omega_0}{1+\beta_0} \;, \tag{2.7}$$

with $\beta_0=\bar{v}(0)/c$, i.e., they imply a resonance between the atomic transition frequency ω_0 and the Doppler-shifted frequencies of the probe and the pump beams.

As our final step we introduce the so-called universal scaling, well known from the theory of the free-electron laser, and cast the working equations in dimensionless form. For simplicity, we let $k_1\approx k_2\equiv k=\omega/c$, $g_1\approx g_2\equiv g$ and, furthermore, define the dimensionless CARL parameter

$$\rho=\left[\frac{g\sqrt{N}}{\omega_r}\right]^{2/3}\propto\left[\frac{N}{V}\right]^{1/3} \;, \tag{2.8}$$

where $\omega_r=2\hbar k^2/m$ is the single-photon recoil frequency shift [9], the scaled time τ, and the new dependent variables P_j and $A_{1,2}$ according to the definitions

$$\tau=\omega_r\rho t \;, \quad P_j=\frac{\delta p_j}{\hbar k\rho} \;, \qquad A_{1,2}=\frac{a_{1,2}^0}{\sqrt{N\rho}} \quad (A_2 \text{ real for definiteness}) \;. \tag{2.9}$$

The final form of the CARL equations of motion is

$$\frac{d\theta_j}{d\tau}=P_j \;, \tag{2.10a}$$

$$\frac{dP_j}{d\tau}=-A_1^*e^{-i\theta_j}S_j-A_1e^{+i\theta_j}S_j^*+2A_2\text{Re}S_j \;, \tag{2.10b}$$

$$\frac{dA_1}{d\tau}=i\Delta_{2,1}A_1+\frac{1}{N}\sum_{j=1}^{N}S_je^{-i\theta_j} \;, \tag{2.10c}$$

$$\frac{dS_j}{d\tau}=\frac{i}{2}(P_j+2\Delta_{2,0})S_j-\rho D_j(A_1e^{i\theta_j}+A_2)-\Gamma_\perp S_j \;, \tag{2.10d}$$

$$\frac{dD_j}{d\tau}=[2\rho(A_1^*e^{-i\theta_j}+A_2)S_j+\text{c.c.}]-\Gamma_\parallel(D_j-D_j^{\text{eq}}) \;, \tag{2.10e}$$

where the remaining parameters are defined as follows:

$$\Delta_{2,1}=\frac{\delta_{2,1}}{\omega_r\rho} \;, \quad \Delta_{2,0}=\frac{\delta_{2,0}}{\omega_r\rho} \;, \tag{2.11a}$$

$$\Gamma_\perp=\frac{\gamma_\perp}{\omega_r\rho} \;, \quad \Gamma_\parallel=\frac{\gamma_\parallel}{\omega_r\rho} \;. \tag{2.11b}$$

Equations (2.10) form a closed, self-consistent set of equations for the internal and translational atomic degrees of freedom, coupled to the driving field A_2 and the probe field A_1, whose amplification is the main objective of this work. In arriving at this result, as already mentioned, we have assumed $k_1\approx k_2\equiv k$; if $k_1\neq k_2$, Eqs. (2.10) are still valid in the so-called Bambini-Renieri frame [10] moving with a verlicity $v_{r,1}$ [see Eq. (2.6c)], where the transformed frequencies coincide. We note that for a nearly resonant interaction, i.e., $\delta_{2,1}\approx 0$, it follows that $\bar{v}(0)\approx v_{r,1}$. We distinguish two cases:

(i) Nonrelativistic particles [$\bar{v}(0)\ll c$]; in this case we have $\omega_1\approx\omega_2$ and our equations are valid in the laboratory frame.

(ii) Relativistic particles [$\bar{v}(0)\approx c$]; in this case it follows that

$$\omega_1=\frac{c+v_{r,1}}{c-v_{r,1}}\omega_2=\frac{1+\beta_0}{1-\beta_0}\omega_2\approx 4\gamma^2\omega_2 \;, \tag{2.12}$$

where $\gamma=(1-\beta_0^2)^{-1/2}$; hence ω_1 can be considerably larger than ω_2. Thus, our formulation can also account for the dynamics of relativistic particles; of course, in this case one needs an additional Lorentz transformation of Eq. (2.10) back to the laboratory frame. This additional step is straightforward and will be discussed elsewhere.

Equations (2.10d) and (2.10e) are the atomic Bloch equations, generalized for the inclusion of the atomic translational motion. In addition to the familiar detuning term $\Delta_{2,0}S_j$ in the polarization equation (2.10d), one may note the appearance of the time-dependent detuning contribution $P_jS_j/2$ resulting from the recoil suffered by the atoms under the action of the driving and probe fields. If we ignore the probe field ($A_1=0$), Eqs. (2.10) describe the usual cooling process for times long compared to $\Gamma_\perp^{-1}$ and $\Gamma_\parallel^{-1}$. If, instead, we set $A_2=0$ and $S_j=1$, for all j, the modified equations (2.10a)–(2.10c) reduce to the traditional FEL equations.

The structure of Eq. (2.10c) indicates that the probe field A_1 can be amplified in the presence of an atomic polarization (but without the need for an initial population inversion) if the phase of the polarization has the appropriate value and if the atomic positions are properly bunched. If the scaled position variables are uniformly distributed between 0 and 2π, just as one has at the beginning of the evolution, no macroscopic field source exists even if the atomic polarization variables S_j are maximized for all values of j because

$$\sum_{j=1}^{N} e^{-i\theta_j}=0 . \tag{2.13}$$

Equations (2.10) for a wide range of parameters predict the development of an exponential instability for the probe field and for the bunching parameter

$$b=\left|\frac{1}{N}\sum_{j=1}^{N} e^{-i\theta_j}\right| . \tag{2.14}$$

The result of this instability is the growth of a macroscopic field and the spontaneous creation of a longitudinal spatial structure in the initially uniform atomic beam with a periodicity that matches the wavelength of the reflected field. This type of behavior can be easily demonstrated by numerical integration of Eqs. (2.10) as we discuss in the next section for several parameter settings of interest.

III. SOLUTION OF THE MODEL EQUATIONS AND DISCUSSION OF THE RESULTS

Ideally, it would be useful to preface a survey of the numerical solutions with a formal linear stability analysis of the problem, not only as a guide to the selection of the parameters but also, and especially, to illuminate the physical origin of the amplification process. In the case of an ordinary laser (this is true also for a FEL), the initial state of the system is a stationary state which becomes unstable at threshold and yields an exponential growth of the field following any initial perturbation.

The initial state of the CARL, instead, is not a stationary state, because Eq. (2.10d) at $\tau=0$ takes the form

$$\left.\frac{dS_j}{d\tau}\right|_{\tau=0}=-\rho A_2\neq 0 . \tag{3.1}$$

Nevertheless, it is still possible to acquire useful information on the physical nature of the amplification process and, especially, on the response of the driven atoms to a weak probe with the help of the short-time evolution of the probe intensity or, more precisely, of the quantity

$$G(\tau,\Delta_{21})=\frac{|A_1(\tau)|^2-|A_1(0)|^2}{|A_1(0)|^2} , \tag{3.2}$$

over a suitable range of values of the detuning parameter $\Delta_{2,1}$. When viewed as a function of $\Delta_{2,1}$, for a fixed value of τ and of the remaining system parameters, G can be interpreted, loosely speaking, as a kind of probe gain–absorption spectrum. This interpretation becomes rigorously correct if the probe intensity varies exponentially as $|A_1(\tau)|^2=|A_1(0)|^2\exp[\alpha(\Delta_{21})\tau]$, where α is a rate constant, and if $\alpha\tau\ll 1$; however, even if these conditions are not satisfied, this quantity continues to offer useful insight into the mechanism of amplification, as we now show.

Figure 1 displays a typical frequency dependence of the "gain spectrum" for $\Delta_{2,0}<0$ and for two selected values

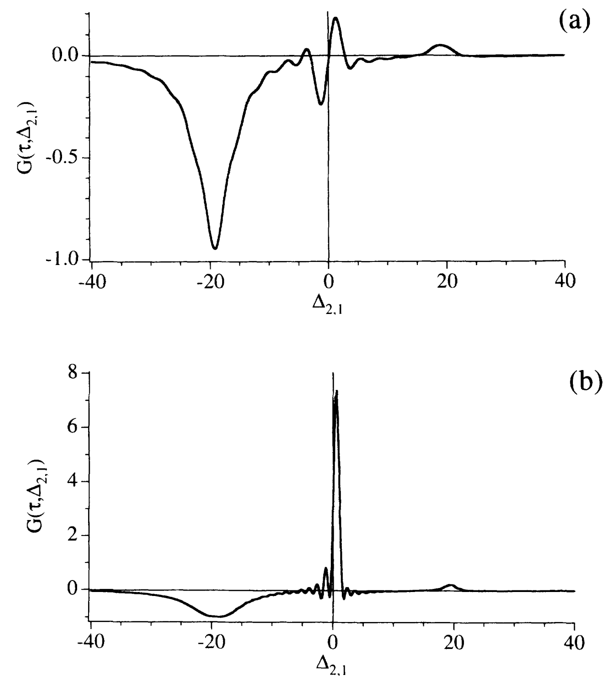

FIG. 1. Frequency dependence of the gain spectrum $G(\tau,\Delta_{2,1})$ [Eq. (3.2)] for (a) $\tau=2$ and (b) $\tau=5$. The parameters chosen for the simulation are $\Gamma=1, \rho=3, A_2=2, \Delta_{2,0}=-15$.

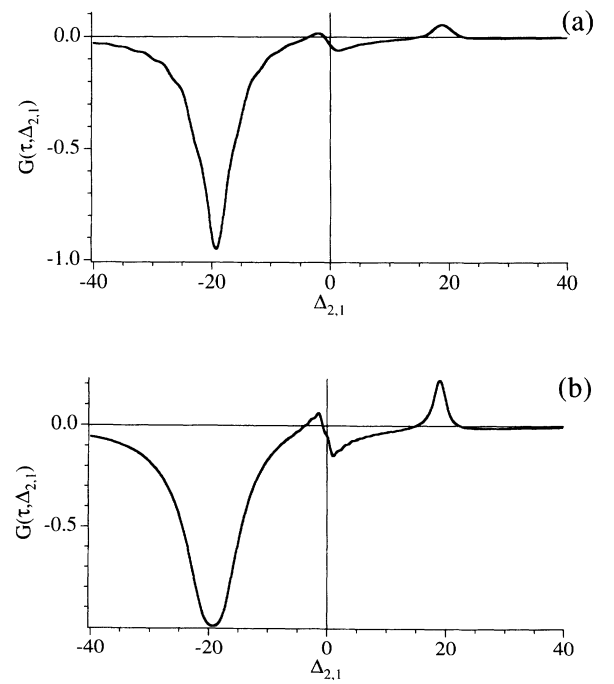

FIG. 2. Frequency dependence of the gain spectrum $G(\tau,\Delta_{2,1})$ [Eq. (3.2)] in the limit of no atomic recoil, i.e., with the momentum P_j of each atom set (artificially) equal to zero in the CARL equations (2.10). Curve (a) corresponds to $\tau=2$ and curve (b) to $\tau=5$. The parameters chosen for this simulation are the same as for Fig. 1, i.e., $\Gamma=1, \rho=3, A_2=2, \Delta_{2,0}=-15$.

of τ [11]. For $\tau=2$ [Fig. 1(a)] three main features are immediately apparent: an absorption dip to the left of the resonance ($\Delta_{2,1}=0$), a small gain peak (Raman peak) shifted from the resonance by the amount $(A_2^2+\Delta_{2,0}^2)^{1/2}$, i.e., the effective Rabi frequency of the driving field, and a dispersionlike feature in the neighborhood of $\Delta_{2,1}=0$, which we identity as the small signal Madey profile. As time progresses, the Madey structure, which is initially antisymmetric as a function of $\Delta_{2,1}$, develops a symmetric shape and grows quite large even during the short time of this simulation, indicating that probe amplification is possible in this frequency range.

The Raman gain and absorption profile displayed in Fig. 1(a) are reminiscent of the corresponding features of the probe spectrum of a stationary driven two-level atom [5] and, indeed, if we solve Eq. (2.10) under the (artificial) constraint $P_j(\tau)=0$, we obtain the results displayed in Fig. 2, which, for short times, are not only qualitatively but also quantitatively very similar to those of Fig. 1, apart from the Madey structure which is associated with the effects of recoil and is replaced, in the case of stationary atoms by the so-called Rayleigh feature. In the limit when the atomic recoil is neglected (we refer to this situation as the Mollow limit) the individual spectral components evolve only slightly during a comparable time interval. Thus, it would appear that preventing the atoms from recoiling (hence, preventing the development of the grating structure) removes a major physical component of the CARL amplification process.

When the atoms are driven resonantly by the external pump ($\Delta_{2,0}=0$), as shown in Fig. 3, the gain spectrum becomes more symmetric, and the gain sidebands reflect qualitatively the characteristic shape predicted by the Mollow theory, which we show for completeness in Fig. 4 under the constraint $P_j(\tau)=0$. However, unlike the Mollow spectrum, the CARL gain profile of Fig. 3 shows again the antisymmetric telltale sign of recoil effects near $\Delta_{2,1}=0$. There is also some significant lack of symmetry in the overall shape of the CARL spectrum even under resonant conditions, which we interpret as the consequence of the recoil-induced detuning in the polarization equation (2.10d).

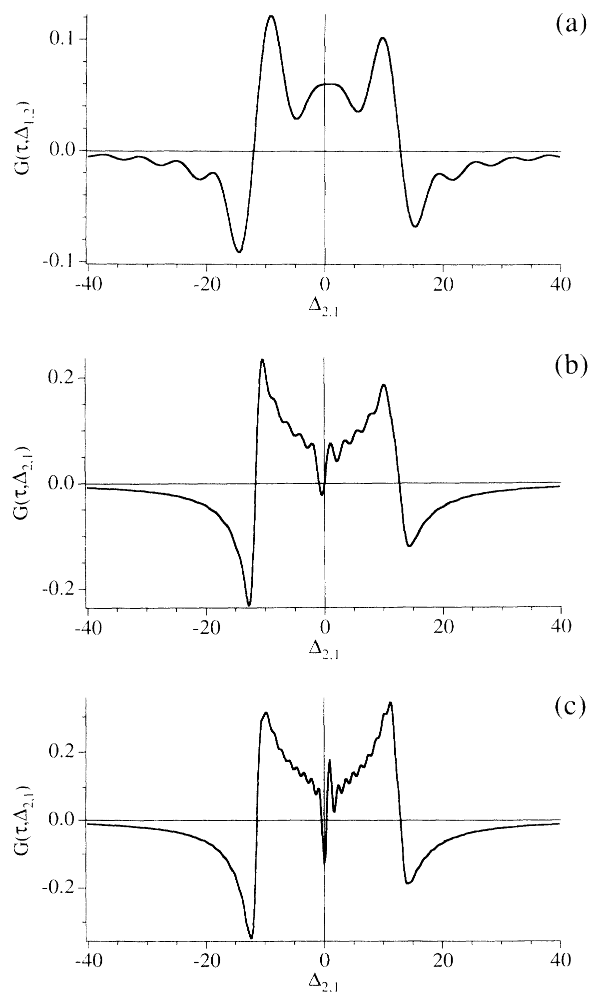

FIG. 3. Frequency dependence of the gain spectrum $G(\tau,\Delta_{2,1})$ [Eq. (3.2)] for (a) $\tau=1$, (b) $\tau=3$, and (c) $\tau=5$, and a resonant pump field ($\Delta_{2,0}=0$). The parameters chosen for this simulation are $\Gamma=1, \rho=3, A_2=2$.

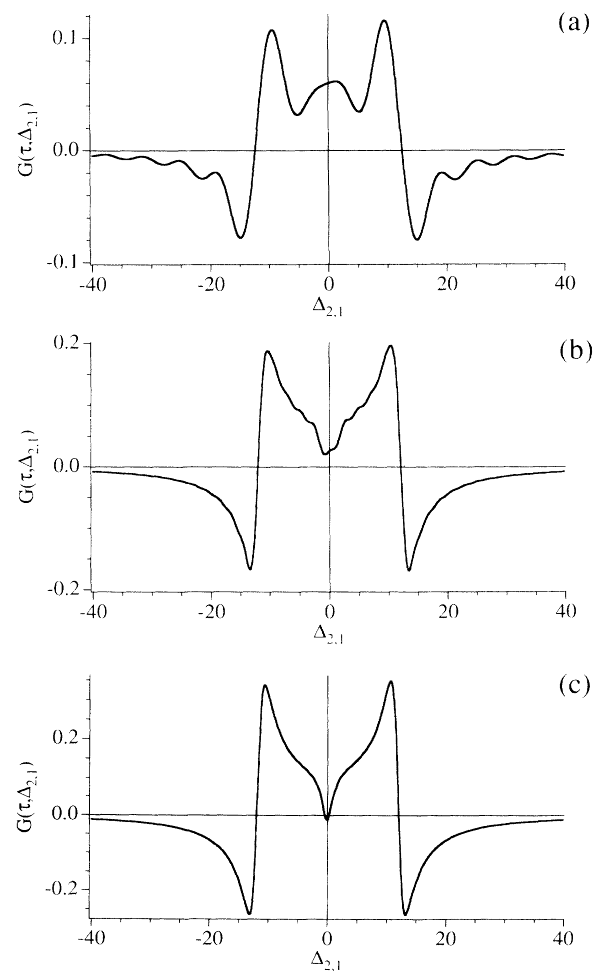

FIG. 4. Frequency dependence of the gain spectrum $G(\tau,\Delta_{2,1})$ [Eq. (3.2)] for a resonant pump field ($\Delta_{2,0}=0$) in the limit of no atomic recoil for (a) $\tau=1$, (b) $\tau=3$, and (c) $\tau=5$. The parameters chosen for this simulation are the same as for Fig. 3, i.e., $\Gamma=1, \rho=3, A_2=2, \Delta_{2,0}=0$.

We now turn out attention to the long-time behavior of the solutions of Eq. (2.10). A typical result is shown in Fig. 5 for the same parameters used in Fig. 1 in the neighborhood of $\Delta_{2,1}=0$. Figure 5(a) displays the temporal evolution of the probe intensity and the buildup of a macroscopic pulse after a characteristic period of lethargy, which is the signature of the developing grating structure. Unlike most temporal instabilities in laser physics, which are characterized by an initial exponential growth, the probe intensity in our case evolves in a rather complicated and, apparently, not exponential way during the first few units of time (roughly, $0<\tau<8$ in this figure) and then undergoes an exponential growth, as shown in the range $8<\tau<15$ of the semilogarithmic inset. The degree of spatial organization of the atoms is surprisingly large, as evidenced in Fig. 5(b) by the maximum value of the bunching parameter (≈ 0.8). In Fig. 5(c) we show the temporal evolution of the average atomic momentum: during the buildup phase of the probe field and immediately after the creation of a macroscopic polarization (indicated by the small-scale Rabi oscillations at the start of the trace), the average atomic momentum decrease almost linearly as a result of the retarding action of the driving field A_2. When the probe field begins to grow, the deceleration of the atomic motion proceeds at a considerably larger rate, showing that the probe amplification process evolves at the expense of atomic kinetic-energy loss. The subsequent acceleration of the atoms, following the peak of the amplified pulse, is apparently caused by the copropagating probe field, which is now sufficiently large to produce an appreciable ponderomotive force; the transfer of energy back to the atoms is the immediate cause for the decrease of the probe intensity and the eventual formation of the first amplified pulse. Figure 5(d) displays the evolution of the real and imaginary parts of the average polarization. The initial transient is characterized by rapid Rabi oscillations, which are followed by a period of lethargy and by the telltale signs of probe amplification. Here the most significant feature is that, apart from the initial oscillatory phase, the absolute value of the real part of the average polarization is much smaller than that of the corresponding imaginary part. This is indicative that the dispersive part of the atomic response plays a more significant role than the absorptive component. We can mention at this point that the corresponding solution for $\Delta_{2,1}\approx 20$ [Raman gain peak in Fig. 1(b)] also displays probe amplification, with a lower peak intensity, while for $\Delta_{2,1}\approx -20$ the initial probe field is absorbed.

In order to gain some additional understanding into the physical principles that govern the CARL process, it is convenient to focus on the evolution in a regime where the internal degrees of freedom D_j and S_j can be eliminated adiabatically. In this limit $(dS_j/d\tau,\ dD_j/d\tau\approx 0)$ we have

$$S_j\approx -\frac{\rho}{B_j}(A_1e^{i\theta_j}+A_2)\left[\Gamma+\frac{i}{2}(P_j+2\Delta_{2,0})\right], \tag{3.3a}$$

$$D_j\approx \frac{1}{B_j}[\Gamma^2+\tfrac{1}{4}(P_j+2\Delta_{2,0})^2], \tag{3.3b}$$

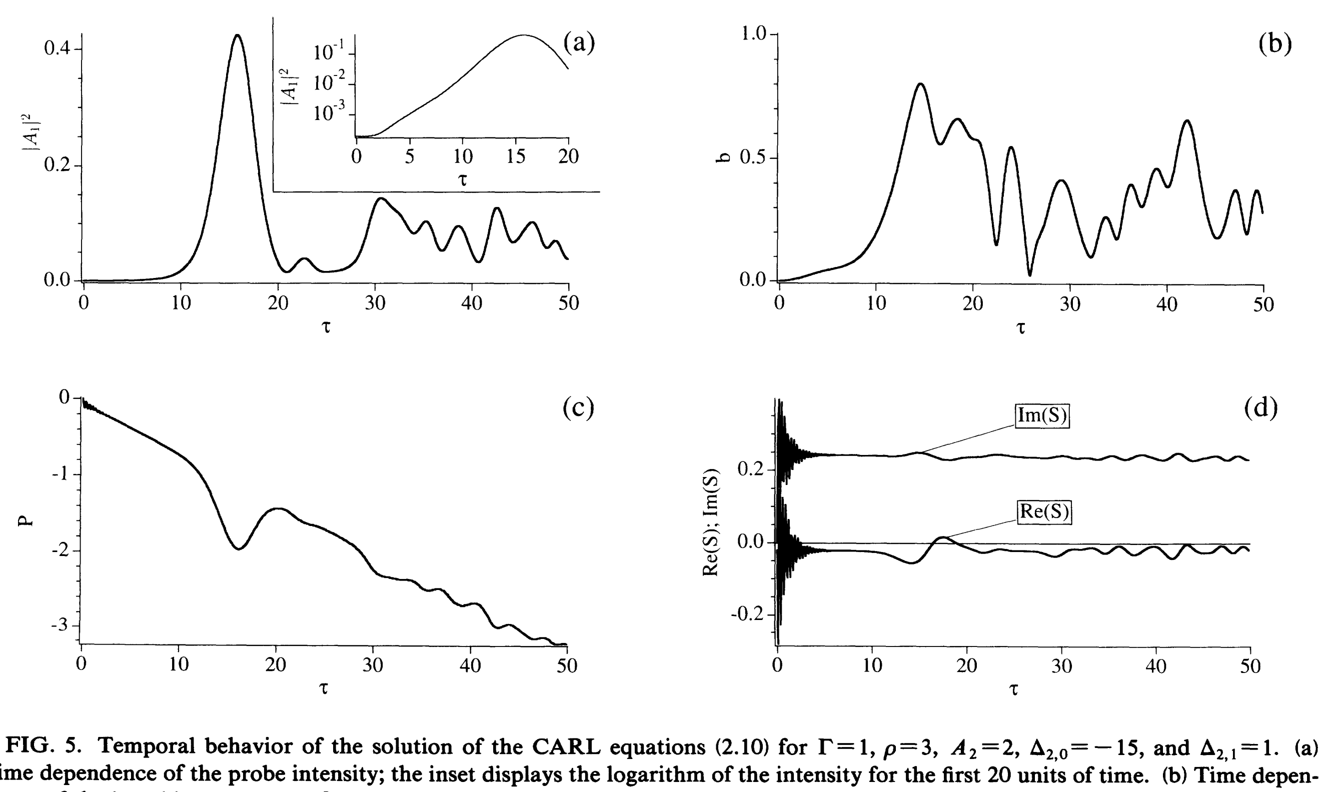

FIG. 5. Temporal behavior of the solution of the CARL equations (2.10) for $\Gamma=1$, $\rho=3$, $A_2=2$, $\Delta_{2,0}=-15$, and $\Delta_{2,1}=1$. (a) Time dependence of the probe intensity; the inset displays the logarithm of the intensity for the first 20 units of time. (b) Time dependence of the bunching parameter [Eq. (2.14)]. (c) Time dependence of the average atomic momentum P. (d) Time dependence of the real and imaginary parts of the average polarization S.

where

$$B_j=[\Gamma^2+\tfrac{1}{4}(P_j+2\Delta_{2,0})^2]+4\rho^2|A_1e^{i\theta_j}+A_2|^2 , \qquad (3.3c)$$

and where we have assumed $\Gamma_\perp=\Gamma_\parallel\equiv\Gamma$ for simplicity. With the help of Eqs. (3.3), Eqs. (2.10a)–(2.10c) take the form

$$\frac{d\theta_j}{d\tau}=P_j , \qquad (3.4a)$$

$$\frac{dP_j}{d\tau}=\frac{2\rho}{B_j}\left[\Gamma|A_1|^2-\Gamma|A_2|^2 + \frac{i}{2}A_2(P_j+2\Delta_{2,0})(A_1^*e^{-i\theta_j}-A_1e^{i\theta_j})\right] , \qquad (3.4b)$$

$$\frac{dA_1}{d\tau}=i\Delta_{2,1}A_1-\frac{\rho}{N}\sum_{j=1}^{N}\frac{1}{B_j}(A_1+A_2e^{-i\theta_j}) \times\left[\Gamma+\frac{i}{2}(P_j+2\Delta_{2,0})\right] . \qquad (3.4c)$$

We see at once that, in the special case $A_1=0$, the adiabatic equation (3.4b) describes the ordinary cooling process and that, in the limit of large driving fields, the optimum rate of momentum decrease is $\Gamma/(2\rho)$. Because a large decrease of the atomic momentum through the normal cooling process also decreases the available kinetic energy that could be used in the amplification of the probe field, it is desirable to minimize this effect. One obvious way to do so is by selecting small values of the ratio $\Gamma/(2\rho)$ or, equivalently, by imposing the condition $\gamma \ll \omega_r\rho^2$, where $\gamma\equiv\gamma_\perp=\gamma_\parallel$.

A proof of this statement is shown in Figs. 6(a)–6(c). The smaller peak power of the amplified probe for the case $\Gamma=2$ [Fig. 6(b)] indicates that a significant loss of atomic momentum has taken place through the ordinary cooling mechanism, as one can confirm directly by inspection of the temporal behavior of the average momentum [Fig. 6(c)]. The duration of the lethargy and the size of the bunching parameter (not shown) are essentially the same in both cases but, as the probe field begins to grow, the average momentum is significantly smaller in the case $\Gamma=2$ than for $\Gamma=0.1$, as one should expect.

Note that, while our qualitative statement on the optimum selection of $\Gamma/(2\rho)$ is made on the basis of rate equations arguments, the results shown in Figs. 6 have been obtained from the numerical solution of the exact equations of motion (2.10). In fact, quite generally, we have noted that the predictions drawn on the basis of Eqs. (3.4) hold accurately, at least in a qualitative sense, also for the exact equations of motion, provided that the decay rate Γ is sufficiently large to justify the use of the adiabatic approximation. An example is shown in Fig. 7.

Another useful scaling relation that can be verified by direct inspection of Eqs. (3.4) is the approximate invariance of the amplification buildup process for constant values of the cooling rate $\Gamma/(2\rho)$ and of the product ρA_2. This invariance holds if $|A_1|$ and $|\Delta_{2,0}|$ are

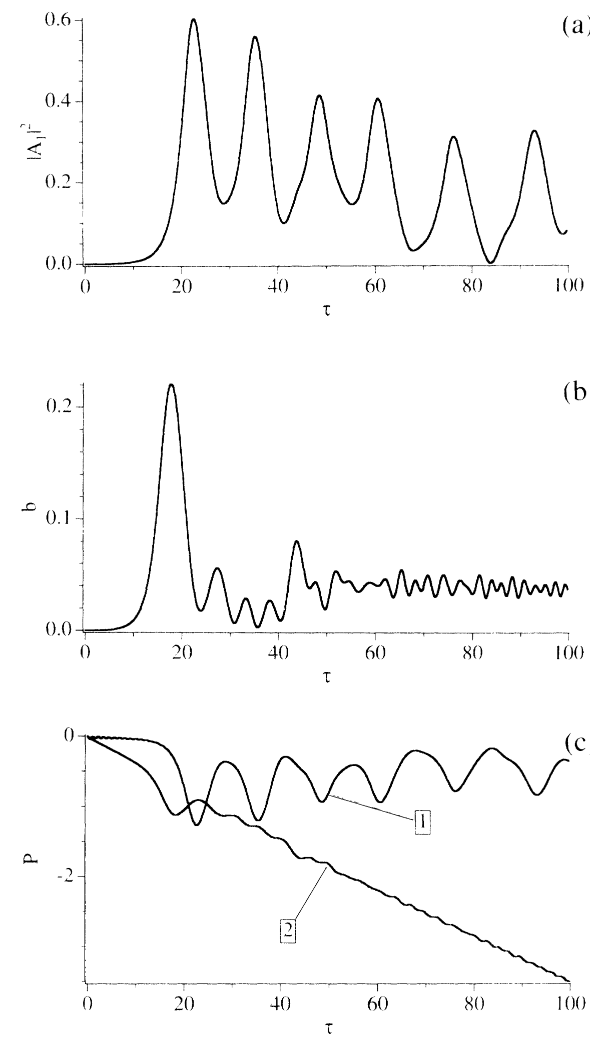

FIG. 6. Effect of the atomic momentum and energy loss due to the ordinary cooling effect. (a) Time dependence of the probe intensity for $\Gamma=0.1$, $\rho=3$, $A_2=2$, $\Delta_{2,0}=-35$, and $\Delta_{2,1}=0.5$. (b) Time dependence of the probe intensity for the same parameters chosen in (a), except for $\Gamma=2$. The larger atomic cooling is responsible for a significant decrease of the maximum probe intensity. (c) Time dependence of the average momentum P for the two selected values of the decay rate Γ.

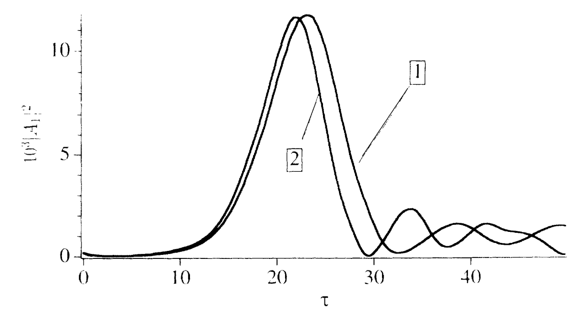

FIG. 7. Comparison between the time dependence of the probe intensity calculated from the exact CARL equations (2.10) (curve 1) and their rate equations limit (3.4) (curve 2). The parameters chosen for this simulation are $\Gamma=4$, $\rho=10$, $A_2=0.5$, $\Delta_{2,0}=0$, and $\Delta_{2,1}=1$.

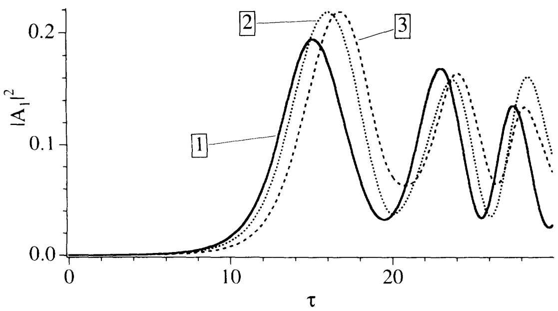

FIG. 8. Approximate invariance of the time evolution of the probe intensity for physical situations characterized by the same cooling rate $\Gamma/2\rho$ and by the same product ρA_2. The detuning parameters chosen for this simulation are $\Delta_{2,0}=-10$ and $\Delta_{2,1}=1$. The remaining parameters are curve 1: $\rho=\frac{10}{3}$, $\Gamma=\frac{2}{3}$, $A_2=3$; curve 2: $\rho=5$, $\Gamma=1$, $A_2=2$; curve 3: $\rho=10$, Γ_2, $A_2=1$.

sufficiently smaller than ρA_2, as one can easily verify from Eqs. (3.4b), (3.4c), and (3.3c). A test of this statement is shown in Fig. 8 for different selections of the parameters Γ, ρ, and A_2.

IV. COMMENTS AND CONCLUSIONS

By taking into account the translation degrees of freedom of the active medium, we have described a mechanism that can lead to the exponential amplification of a weak probe. Roughly speaking, we can interpret the process of amplification as evolving in two steps: first, the external field creates a weak gain profile in the frequency response of a collection of independent driven atoms and begins the buildup of a spatial structure with the help of the atomic recoil; next the probe, whose carrier frequency lies within a selected gain region of the active medium, undergoes exponential amplification. The role of the atomic recoil is essential to this process: not only is it the cause of the emergence of the spatial grating pattern, but it also reinforces the coherent growth of the signal to be amplified as energy is transferred form the atoms to the probe field.

An alternative way of interpreting the probe amplification is to view it as the reflection of the driving field from the moving grating pattern or as a kind of coherent scattering from the bound states of the atom. If the active medium is stationary, apart from the thermal motion such as one has in an ordinary gas cell or in optical molasses, the frequency of the reflected light may be shifted from the frequency of the pump field, at most by a small amount of the order of the effective Rabi frequency of the pump. If the atoms, instead are injected at relativistic speed into the interaction region, the reflected signal can be upshifted to a frequency of the order of $4\gamma^2\omega_2$, well into the short-wavelength region of the electromagnetic spectrum if the relativistic factor γ is sufficiently greater than unity.

An experiment has been reported recently by Courtois and co-workers [7], showing a small-gain regime in a cold gas of cesium atoms. This experiment employed nearly copropagating pump and probe beams, with $\Delta_{2,0}<0$, and yielded an antisymmetric gain profile with a shape similar to the short-time Madey profile described in Fig. 1(a). The experimental structure displays zero gain at a frequency $\Delta_{2,0}=0$ (in our notation) and a functional form that is the derivative of the thermal Gaussian velocity distribution of the atoms. The spatial bunching they infer arises from the partial optical trapping produced by the two applied fields. In contrast, the Madey gain in the short-time limit has the functional form of the derivative of the square of the sinc function that arises from the pendulum dynamics [6]. Furthermore, the exponential regime predicted in our paper is characterized by a large gain in the neighborhood of $\Delta_{2,1}=0$ [see, for example, Figs. 5(a) and 6(a)]. Therefore, it appears that these experimental results are not a verification of the effects discussed here, especially because we see no evidence of collective self-bunching due to the self-consistent field generated by the bunching itself.

If this identification is correct, it would appear that the selected configuration cannot lead easily to the observation of the exponential amplification regime. Nevertheless, in our opinion, the experiments reported by Verkerk *et al.* represent a significant accomplishment as a demonstration of the CARL gain mechanism in the small gain regime.

We conclude with a preliminary estimate of a few relevant parameters for a gas of rubidium atoms driven at the $5\,^2S_{1/2}-5\,^2P_{3/2}$ resonance line ($\lambda=780.24$ nm). For this atomic transition and counterpropagating pump and probe beams, the single-photon recoil frequency shift is $\omega_r=9.6\times10^4$ sec^{-1} and the dimensionless CARL parameter is $\rho=4.2\times10^{-3}n^{1/3}$, where n is the gas density measured in units of m^{-3}. Thus, it follows that the collective linewidth $\omega_r\rho$ has the approximate value $4\times10^2 n^{1/3}$ sec^{-1}. For a gas density of 10^{18} atoms/m^3, we have $\rho=4.2\times10^3$ and $\omega_r\rho=4\times10^8$ sec^{-1}.

Our numerical solutions show a wide range of lethargy times and output pulse durations, in addition to those displayed in the figures. If we select $\tau=20$ as a characteristic dimensionless evolution time, this corresponds to 50 nsec for the rubidium parameters listed above. We may also mention that, with a full width at half maximum, $\Delta\nu=6$ MHz and a corresponding polarization relaxation rate $\gamma_\perp=\pi\Delta\nu=1.9\times10^7$ sec^{-1}, the condition for negligible cooling $\gamma_\perp\ll\omega_r\rho^2$ is very well satisfied.

In this paper, we have not considered the role played by the velocity spread of the active medium, which we have implicitly assumed to be made up of monoenergetic atoms. Qualitatively, however, it is reasonable to expect that the assumption of negligible velocity spread should continue to be valid as long as the associated spread in frequency shifts remains smaller than the collective linewidth $\omega_r\rho$ or about 64 MHz (4×10^8 rad/sec) for the numerical example given above. This issue, as well as additional consequences of our theoretical analysis, will be analyzed elsewhere.

ACKNOWLEDGMENTS

We are grateful to Professor N. B. Abraham and Professor J. R. Tredicce for useful discussions and critical comments.

[1] R. Bonifacio and L. De Salvo, Nucl. Instrum. Methods Phys. Res. Sec. A **341**, 360 (1994).

[2] We use the word "atoms" in a generic sense; any two-level system will do for our purposes, although in practice we may be concerned with charged particles, ions for example, especially if the atoms are required to travel at high speed.

[3] R. Bonifacio, C. Pellegrini, and L. M. Narducci, Opt. Commun. **50**, 373 (1984).

[4] O. Kocharovskaya and Ya. I. Khanin, Pisma Zh. Eksp. Teor. Fiz. **48**, 581 (1988) [JETP Lett. **48**, 630 (1988)]; S. E. Harris, Phys. Rev. Lett. **62**, 1033 (1989); M. O. Scully, S.-Y. Zhu, and A. Gavrielides, *ibid.* **62**, 2813 (1989); L. M. Narducci, H. M. Doss, P. Ru, M. O. Scully, S.-Y. Zhu, and C. H. Keitel, Opt. Commun. **81**, 379 (1991).

[5] B. R. Mollow, Phys. Rev. A **5**, 1522 (1972); **5**, 2217 (1972); F. Y. Wu, S. Ezekiel, M. Ducloy, and B. R. Mollow, Phys. Rev. Lett. **38**, 1077 (1977).

[6] J. M. Madey, Nuovo Cimento **50**, 64 (1979); see also R. Bonifacio, G. T. Moore, M. O. Scully, and P. Meystre, Phys. Rev. A **21**, 2009 (1980).

[7] J.-Y. Courtois, G. Grynberg, B. Lounis, and P. Verkerk, Phys. Rev. Lett. **72**, 3017 (1994).

[8] The final equations of motion involve ordinary c-number functions, which we denote with the same symbols as the corresponding operators because no ambiguity is likely to occur.

[9] The parameter ρ is a measure of the collective effects; in fact, $g\sqrt{N}$ is the collective spontaneous Rabi frequency of an ensemble of N two-level atoms [see, for example, R. Bonifacio, P. Schwendimann, and F. Haake, Phys. Rev. A **4**, 382 (1971); **4**, 854 (1971)].

[10] A. Bambini and A. Renieri, Opt. Commun. **29**, 24 (1974); A. Bambini, A. Renieri, and S. Stenholm, Phys. Rev. A **19**, 2013 (1979).

[11] We have carried out the numerical integration of Eqs. (2.10) by a standard fourth-order Runge-Kutta routine. In these calculations we have selected as initial conditions $P_j=0$, $D_j=1$ (for all values of j), θ_j uniformly distributed between 0 and 2π, and $A_1(0)=\varepsilon(1+i)$, $S_j=\varepsilon'(1+i)$, where ε and ε' are small numbers of the order of 10^{-2} and 10^{-3}, respectively. Furthermore, in order to simulate the start-up noise, we have added small Gaussian random numbers with zero mean to the initial values of θ_j and S_j.